Composites Science and Technology 235 (2023) 109952

Contents lists available at ScienceDirect

Composites Science and Technology

journal homepage: www.elsevier.com/locate/compscitech

Fabrication of chitosan-flax composites with differing molecular weights and its effect on mechanical properties

Amrita Rath [a], Benjamin Grisin [b], Tarkes Dora Pallicity [c], Lukas Glaser [b], Jajnabalkya Guhathakurta [d], Nina Oehlsen [a], Sven Simon [d], Stefan Carosella [b], Peter Middendorf [b], Linus Stegbauer [a,*]

[a] Institute for Interfacial Process Engineering and Plasma Technology IGVP, University of Stuttgart, Pfaffenwaldring 31, 70569, Stuttgart, Germany
[b] Institute of Aircraft Design IFB, University of Stuttgart, Pfaffenwaldring 31, 70569, Stuttgart, Germany
[c] Institute of Engineering Mechanics ITM, Karlsruhe Institute of Technology, Kaiserstraße 10, 76131, Karlsruhe, Germany
[d] Institute of Computer Architecture and Computer Engineering ITI, University of Stuttgart, Universitätsstraße 38, 70569, Stuttgart, Germany

ARTICLE INFO

Keywords:
Bio composites
Natural fiber composites
Mechanical properties
Multiscale material modeling
Biodegradability

ABSTRACT

An aqueous fabrication method is investigated for a composite reinforced with chitosan and flax fibers. The composite is characterized structurally, mechanically and chemically. A strong influence of molecular weight (MW) is identified on the composite properties. A strong fiber-matrix interface, which is associated with porosity and effective fiber impregnation, is achieved by applying low molecular weight (LMW) solution followed by casting using LMW or medium molecular weight (MMW) solution. Porosity is analyzed using μ-CT analysis. Increasing porosity with increasing molecular weight results in a decline of the tensile and flexural properties of the composites. The chitosan-flax composites have a low density compared to synthetic and natural fiber composites, which is a competitive advantage as a replacement material for particle board or plyboard in suspended ceilings, furniture compartments, sports or leisure equipment. A multiscale simulation is carried out to compute the directional effective elastic properties and predicts a potential 21% improvement of the tensile modulus if the process is optimized. This work shows the potential of chitosan-flax composites as a sustainable green material with an aqueous fabrication procedure and useful mechanical properties.

1. Introduction

The current shortage of natural resources and worsening environmental pollution and global warming are leading to a serious crisis [1]. This has encouraged development of sustainable bio composites to displace fossil-based polymer composites as light-weight structural materials. Light-weight structural polymer composites are applied extensively across industries including in the manufacturing of household appliances, sports equipment, transport vehicles, turbine blades, and aircraft parts. Broad applicability of these composites due to their high strength, high stiffness, low cost, and processability with high flexibility in design [2]. However, this performance comes at a high cost as fossil-based polymers add CO_2 emissions by the end of life if not recycled and recycling of polymer composites is both energy intensive and can degrade mechanical properties. Today, most composites are incinerated or transported to landfills at the end of life [3]. There is a dire need for a paradigm shift in structural polymer composites to meet both economic viability and sustainability. Increased use of bio composites could resolve this need by utilizing abundant and inexpensive biomass with advantages of biodegradability, biocompatibility, non-toxicity, renewability, sustainability, and a low carbon dioxide footprint [4–7].

Several efforts have been made in order to replace non-biodegradable composites, including epoxy-carbon or epoxy-glass used in transport vehicles, with partially biodegradable or fully biodegradable alternatives [8–12]. One driving force is the automotive directive guideline of the European Union directing that more than 95% of the total weight of a vehicle have to be reused and recycled in the end-of-life vehicles (ELV) since 2015 [13]. Such newly developed composites are made from natural fibers such as flax, jute, kenaf, cotton, silk or wool in combination with bio-based polymers from sustainable feedstock such as poly-lactic acid (PLA), poly-butylene succinate (PBS) or biogenic

* Corresponding author.
E-mail address: linus.stegbauer@igvp.uni-stuttgart.de (L. Stegbauer).

https://doi.org/10.1016/j.compscitech.2023.109952
Received 16 September 2022; Received in revised form 2 January 2023; Accepted 8 February 2023
Available online 9 February 2023

biopolymers like chitosan [14–19].

Chitosan is derived from chitin, the second most abundant biogenic polymer in the biosphere after cellulose [20]. The annual production of chitin in the biosphere is estimated to be 1000 billion (10^{11}) tons [21]. Chitosan is a linear polysaccharide composed of β-(1–4) linked glucosamine and *N*-acetyl-D-glucosamine units, produced by alkaline deacetylation of chitin [21,22]. It has excellent film-forming properties [23], is fully biodegradable, can be processed in aqueous solutions and is available inexpensively on bulk scale with a range of properties (molecular weight, degree of acetylation, purity) [24,25]. The bulk prices of chitosan (7.6–11.4 € kg^{-1}) are comparable to epoxy resins (5.12 € kg^{-1}), but higher than PP (1.14 € kg^{-1}) (see Table S5). Increased production scale of chitosan would likely lower prices and increase the quality available. (see Table S5 for a comparison in the cost and availability of commonly used resins and fibers).

For a natural fiber material to use in composites, flax fibers are a potential candidate because mechanical properties can be close to glass fibers and the fibers have low density, high specific strength and modulus as well as wide availability in nature [26]. Flax fibers have several industrially relevant functional properties, such as absorbing vibrations and blocking ultraviolet rays [6]. Flax fibers are derived from the stems of flax bast plant. Flax fibers are mainly composed of the polymer cellulose, which is similar to chitosan on a structural level, in which the monomer units are joined by β-(1–4) glycosidic bonds. The difference is the substitution of amino groups on the C2 position in chitosan, while cellulose is substituted by hydroxyl groups at the same position, thus offering effective adhesion and strong interfacial interaction without chemical modification [27,28]. Flax fibers have been widely used in composites with fossil-based polymers as well as biopolymers for the fabrication of products such as hat racks, door and floor panels, glove boxes, seat backs, door claddings, door and boot liners, parcel shelves and spare tire linings to name a few [29–33].

Previously, chitosan has been combined with natural fibers such as flax, sisal, sunflower stem, banana and coconut fibers. Prabhakar et al. have developed a starch/flax fiber composite by reinforcing chitosan using compression technique [34]. The tensile modulus and strength of the composites were 0.66 GPa and 24.03 MPa. A study by Mati-Baouche et al. presented a composite made from crushed particles of sunflower stalks (bark and pith) bound together by chitosan. with a maximum tensile strength and modulus of 0.14 MPa and 60 MPa [35]. In another study, chitosan composite was prepared by using sisal, banana and coir fibers with varied chitosan composition and natural fibers in a mould casting process [36]. The maximum reported tensile strength was 16.96 MPa (3% chitosan with 2% sisal), 17.8 MPa (2.5% chitosan with 1% banana) and 22.5 MPa (3% chitosan with 2% coir).

In all of the above studies, the process yielded mechanical properties which are not competitive to flax/fossil-based polymers composites. A comprehensive study using chitosan and flax fiber that improves the process to yield composites with comparable mechanical performance for structural applications is not yet available in the literature to the best of author's knowledge. This provides a scope for exploration by varying molecular properties and evaluating the impact on mechanical performance.

Here, the bio composite "chitosan-flax" is presented based on chitosan as a biogenic matrix and flax fibers as reinforcement. The bio composite is made by an aqueous-based fabrication technique. The molecular weight, the weight percentage of polymer solution and the drying conditions have been identified as the critical factors affecting the fabrication of such a composite. An extensive analysis of the composite's mechanical, structural, thermal, chemical, optical, and microstructural properties have been elucidated by applying tensile test, bending test, nanoindentation, differential scanning calorimetry (DSC), thermal gravimetric analysis (TGA), UV–Vis spectroscopy, fourier transform infrared spectroscopy (FTIR), scanning electron microscopy (SEM), optical microscopy (OM) and μ-x-ray computed tomography (μ-CT) analysis. Further, a full-field homogenization is performed to predict the elastic properties of the fabricated chitosan-flax, including directional dependency. The limitations of the fabrication process and the material chitosan-flax are highlighted. The results provide design guidelines for material selection and optimization of chitosan-flax composites.

2. Experimental

2.1. Materials

Low molecular weight (LMW) chitosan (5 mPa s batch viscosity and degree of deacetylation (DDA) of 81.1%); medium molecular weight (MMW) chitosan (30 mPa s and DDA of 85.6%) and high molecular weight (HMW) chitosan (386 mPa s and DDA of 90.1%) were purchased from TCI Deutschland GmbH. Woven flax fabric (Depestele Flax plain weave 400 g m^{-2}) has been purchased from Composites Evolution Ltd, UK. Glacial acetic acid (purity >99.9%) as a solvent was purchased from Sigma Aldrich, Germany.

2.2. Formulations

A detailed procedure carried out in the fabrication of chitosan-flax fiber laminate is shown in Fig. 1. To prepare the chitosan-flax composites, three different chitosan solutions, solution 1, solution 2 and solution 3 were prepared.

Solution 1 (Impregnation). 2% w/w LMW chitosan solution was prepared by dissolving 1.04 g of chitosan powder into 50 mL aq. acetic acid, AcOH (20% v/v). The solution was mixed at 3500 rpm in a planetary centrifugal mixer (Hauschild Speedmixer, DAC 150.3 FVZ, Germany) for 15 min to form a homogenous solution. The mixing time can be reduced to half when the chitosan is soaked in acetic acid solution for 12 h followed by speedmixing.

Solution 2 (Solvent casting). 5% w/w (LMW), 2.5% w/w (MMW) and 1% w/w (HMW) chitosan solution was prepared by dissolving 4.85 g, 4.73 g and 4.65 g of chitosan powder into 90 mL, 180 mL and 450 mL aq. acetic acid, AcOH (20% v/v), respectively. A homogenous solution was prepared in a similar way as mentioned for *Solution 1*.

Solution 3 (Gluing). Chitosan solution was prepared to be used as a glue to bind two laminates. 10% w/w (LMW), 5% w/w (MMW) and 1% w/w (HMW) chitosan solution was prepared by dissolving 1.14 g, 539.5 mg, 103.5 mg of chitosan into 10 mL aq. acetic acid, AcOH (20% v/v).

A summary of the control and variable factors for all the solutions is presented in Table S3.

2.3. Sample preparation

2.3.1. Pristine chitosan films

Chitosan films were prepared from three different MW by applying the solvent casting method. LMW (10% w/w), MMW (6% w/w) and HMW (1% w/w) chitosan solutions were prepared by dissolving 10.25 g, 5.89 g and 931 mg chitosan, respectively in 90 mL aq. AcOH (20% v/v) in a speedmixer as discussed in Section 2.2. The solution was poured in a petri dish (120 mm × 120 mm x 17 mm) and dried in the fume hood (450 m^3 h^{-1}) for about 12–15 h till there was no further change in the weight of the films. The average thickness for LMW, MMW and HMW was measured by using a thickness gauge (Mitutoyo 543-415-1 Digimatic Indicator, Type ID-150M, Japan) and measured to be 267.2 μm, 152.4 μm and 97.9 μm, respectively.

2.3.2. General procedure for flax fiber mat impregnation

A flax fiber mat (100 mm × 100 mm, 1 layer) was initially impregnated by placing it inside a petri dish (120 mm × 120 mm x 17 mm) and pouring 50 mL of *solution 1* (2% w/w, LMW, see Section 2.2) on top of them. The petri dish was closed to let the flax fiber mat soak in the

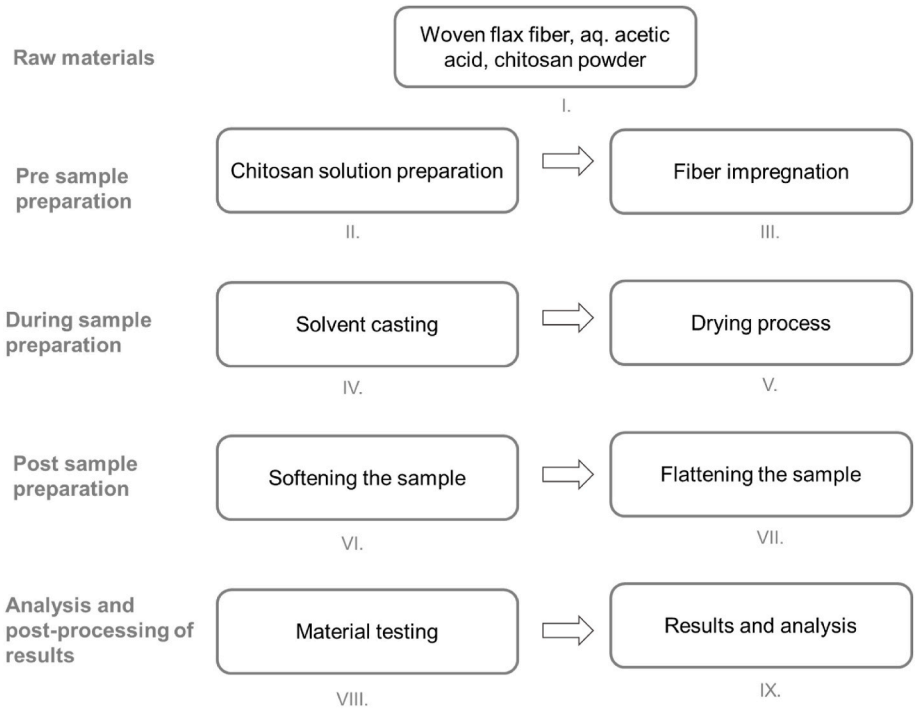

Fig. 1. Fabrication process flow chart for chitosan-flax composite.

solution for 12 h.

2.3.3. LMW chitosan-flax composite

90 mL (5% w/w, LMW, corresponds to 4.5 g overall amount of chitosan) of Solution 2 (see Section 2.2) was poured on the soaked fiber mat. The solution was allowed to dry slowly by placing it inside a well-ventilated room (21.3 °C–25.3 °C, 48%–67% RH) on the bench for 5 days. The average thicknesses of the sample for 10 specimens were measured to be 0.89 mm.

2.3.4. MMW chitosan-flax composite

180 mL (2.5% w/w MMW, corresponds to 4.5 g overall amount of chitosan) of Solution 2 (see Section 2.2) was poured on the petri-dish with the impregnated flax fiber mat (see Section 2.3.2) and allowed to dry for 2 days on the bench, followed by pouring solution 2 (90 mL, 2.5% w/w) when the previous solution was still in liquid state. The solution was allowed to dry slowly by placing it inside a well ventilated room (17.8 °C–19 °C, 26%–43% RH) for 5 days. The average thickness of the sample for 10 specimens were measured to be 0.89 mm.

2.3.5. HMW chitosan-flax composite

450 mL (1% w/w, corresponds to 4.5 g overall amount of chitosan) of Solution 2 (see Section 2.2) was poured in five steps similar to previous procedures. After each pouring step (90 mL, 1% w/w), 2 days were allowed for partial drying, followed by final drying inside a well ventilated room (17.8 °C–19 °C, 26%–43% RH) for 7 days. The average thicknesses of the sample for 10 specimens were measured to be 2.01 mm.

2.3.6. Sample trimming, flattening and final drying

After drying, supernatant polymer film was removed by trimming. For further use, dried samples were treated with steam to soften the polymer. Steam was generated by a household steam iron (Philips, GC4541, Netherlands) and applied to the laminate at 30 cm distance for 5–7 min. The softened samples were flattened by compressing tightly between two metal plates. The samples were air dried by placing them inside a well ventilated room until there was 20% weight reduction in the laminate, followed by final drying until constant weight inside a convection oven (Binder GmbH ED-S 056, Germany), at 35 °C for 3 days.

2.3.7. Double layer chitosan-flax composite

A single layer laminate was formed from the procedure as mentioned above. Two single layer LMW, MMW and HMW laminates were glued together by applying 5 g of LMW (10% w/w), MMW (5% w/w) or HMW (1% w/w) solutions (see Section 2.2, Solution 3) using a spatula and tightly gripped for 5 h. The samples were placed inside a convection oven at 35 °C for 3 days. The double layer laminate was prepared to increase the thickness of the sample required to perform bending tests. Average thickness of the sample for LMW, MMW and HMW laminates were measured to be 1.84 mm, 1.94 mm and 2.93 mm.

2.4. Sample preparation for mechanical testing

The preparation of the film and laminate specimens for tensile, bending and nanoindentation tests is mentioned in details in the *supplementary information* (see *Section 1*).

2.5. Characterization methods

2.5.1. Tensile testing

The tensile testing was performed on pristine chitosan films using a tensile testing machine (Zwick/Roell Z005, Germany) with a 2.5 kN load cell. The tensile tests were performed with a speed of 1 mm min^{-1} for measuring the modulus and 5 mm min^{-1} for measuring the strength and elongation. An initial pre-load of 10 N was applied to remove slack from the load string before a test begins. The testing was carried out on at least 10 samples for each material variation. The tensile testing on the chitosan-flax laminate was performed by using a universal testing machine (Inspekt 20-1, Hegewald and Peschke GmbH, Germany) with a loading cell of 20 kN. All conducted test series were completed after 5 valid measurements. The tests have been concepted according to DIN EN ISO 527-4 whereas the specimen geometry has been adapted due to the

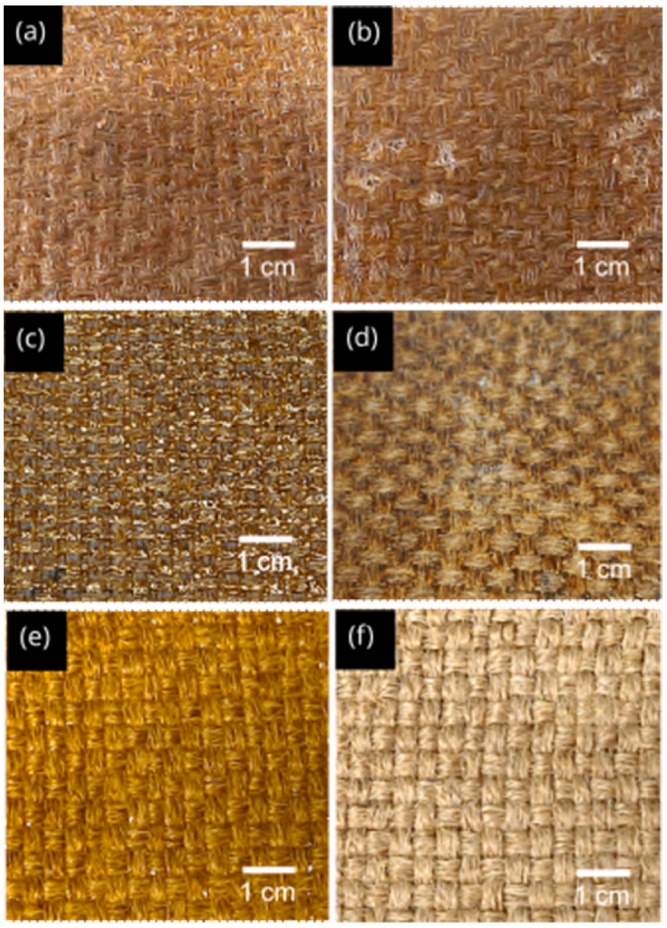

Fig. 2. Image showing an impregnated chitosan-flax laminates: (a) front side and (b) back side with low molecular weight (LMW), (c) front side and (d) back side with medium molecular weight (MMW), (e) front side and (f) back side with high molecular weight (HMW) chitosan solution.

feasible plate size of 100 mm × 100 mm. The test specimen dimensions, length × width × thickness for LMW laminates were 80 mm × 15 mm × 0.89 mm. The thickness for MMW and HMW laminates was 0.89 mm and 2.01 mm, whereas a double layer laminate thickness was 2.31 mm. No tabs have been used. The tests were performed with a speed of 1 mm min^{-1}.

2.5.2. Bending test

The flexural strengths of the composites were evaluated by using a universal testing machine (see above). The four-point bending tests were performed according to DIN EN ISO 14125. The loading rate was set to 2 mm min^{-1}. The two lower supporting fins were set to the span length L = 45.15 mm and the distance between the two upper loading fins were adjusted to (1/3) L. The test specimen dimensions, length x width were 60 mm × 15 mm. The thickness for LMW, MMW and HMW laminates was 1.84 mm 1.94 mm and 2.93 mm. The ratio between length to thickness for LMW, MMW and HMW flax composite samples were 33:1, 32:1 and 20:1, respectively, in order to avoid the specimen failure by shear. The loading supporting and loading fins did not allow rotations around any axis. The testing was carried out on at least 5 samples for measurements on each type.

An Ashby plot is shown in Fig. 3(*d*) to facilitate easy comparison of mechanical properties and design criteria for various engineering applications. These plots are used here to compare chitosan-flax composite performance with other natural [37–41] and synthetic fiber composites [42], all cellulose composites [40,43] and delignified wood composites [44,45]. The properties mentioned in these plots are extracted from various sources [19,37,46–49]. It is to be mentioned that due to limited nature of information available in the literature related to green composites, many of the specific properties could not be plotted. Only for very few materials, their properties were calculated from the reported modulus and strength values.

2.5.3. SEM imaging

The surface morphology and chitosan-flax interface was investigated by using a SEM (Leo-982 and Zeiss Evo15, Germany). The samples were sputtered using a sputter coater (BAL-TEC EVM 030 MCS 010) with a thin layer of gold for 30 s before the analysis to avoid any charging

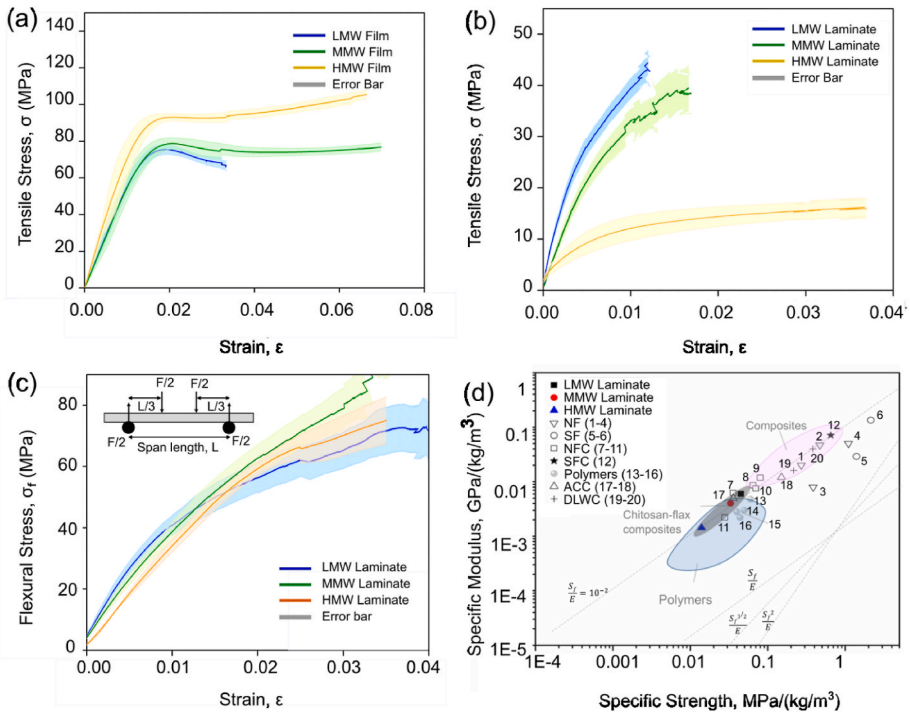

Fig. 3. Plots showing (a) tensile stress vs strain for pure films, (b) tensile stress vs strain for laminates (c) flexural stress vs strain for laminates and (d) specific modulus vs specific strength for chitosan-flax composite in comparison to other engineering materials from tensile tests, dashed line indicates yield strain, S_f/E, elastic energy stored per unit volume for springs, S_f^2/E, and selection for elastic constant, $S_f^{3/2}/E$; Abbreviations: natural fiber (NF); synthetic fiber (SF); natural fiber composites (NFC, Epoxy-Banana [37], PP-Flax [38], PP-Jute [39], Epoxy-Flax [40], PLA-Flax [41]); synthetic fiber composite (SFC, Epoxy-Carbon [39]); all-cellulose composite (ACC, ACC-I [40], ACC-II [44]); delignified wood composite (DLWC, DLW-PMMA [43], DLW-Epoxy [45]); 1. Bamboo, 2. Hemp, 3. Cotton, 4. Flax, 5. E-Glass, 6. Carbon, 7. Epoxy-Banana, 8. PP-Flax, 9. PP-Jute, 10. Epoxy-Flax, 11. PLA-Flax, 12. Epoxy-Carbon, 13. Chitosan, 14. PLA, 15. Epoxy, 16. PP, 17. ACC-I, 18. ACC-II, 19. DLW-PMMA, 20. DLW-Epoxy.

effect. The images were captured at different magnifications with an electron beam acceleration voltage of 5 kV.

2.5.4. OM imaging

The voids/pores on the surface of the chitosan-flax laminates were examined by using an optical microscope (Leitz Metallux 3, Germany) with a magnification in the range from 50 to 500 times. Prior to imaging, embedded samples were ground and polished to obtain a suitable surface quality (see *supplementary information, Section 1.3*). The raw images as obtained from microscopy were used for the porosity analysis by using Image J software (V 1.49, Wayne Rasband, NIH, USA). The percentage of porosity has been calculated as the ratio between the area of black region to white region keeping the total area constant for each of the pictures (see Fig. 5a, c and e). It is to be mentioned that in Fig. 5c and e, voids are not visible clearly, rather larger pores appear to be filled by the resin during sample preparation process (see *supplementary information, Section 1.3*). To reconfirm that, nanoindentation has been performed on these regions and the modulus of elasticity has been determined to be 3–3.5 GPa, which is similar to the modulus of the acrylic resin that is being used here as an embedding medium for sample preparation.

2.5.5. μ-CT

μ-x-ray computed tomography is a 3D non-destructive measurement technique which is capable of measuring the outer as well as the inner features of the sample. During the scan, the sample is rotated by 360° over several thousand steps and corresponding 2D images are captured. These images, called as projections, are then fed into a 3D reconstruction algorithm to generate a 3D volume of the sample being measured. In this work, a CT Scanner with a 225 kV, 225 W microfocus X-ray source, a detector with 3200 × 2304 pixels (pixel pitch of 120 μm) and a DRZ plus scintillator was used. The *X*-ray settings were set to 80 kV, 6 W with an exposure time of 2.8 s and 4500 projections. The 3D reconstructed volume resolution was 1.6 μm. The volumes were then analyzed with VGSTUDIOMAX for porosity analysis. Pores have been counted to a maximum pore volume of 0.0135 mm^3 and 0.088 mm^3 for LMW and MMW laminates.

The shape of the voids as measured by different descriptors, like sphericity and compactness are explained in details in *supplementary information* (*Section 2.13*).

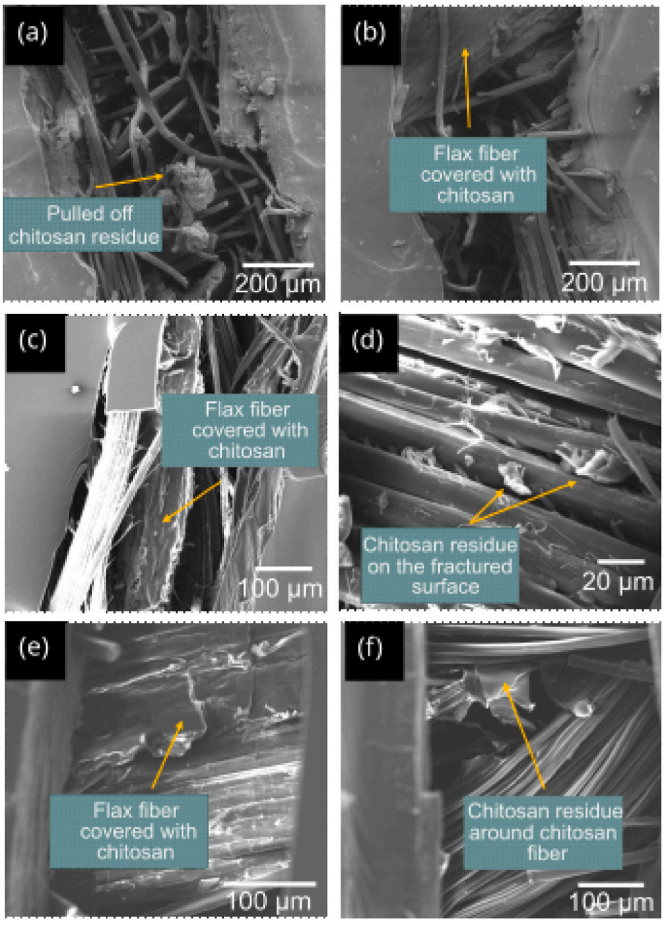

Fig. 4. Scanning electron microscope (SEM) image of fiber/matrix interface for (a) and (b) LMW laminate, (c) and (d) MMW laminate and (e) and (f) HMW laminate for fractured bending test specimens.

2.5.6. Multiscale modeling of chitosan-flax laminate

Microscopic images (Figure S11a and Fig. 5a) show distinguishable features at microscale and mesoscale. Microscale (10–20 μm) features show the distribution of elementary fibers. Mesoscale (2–3 mm) features include fiber bundles with an ellipsoidal shape. In view of this, a two-scale homogenization is used in computing the effective elastic properties of the LMW laminate [50]. Standard tools and methodology used in homogenization are described in *supplementary information* (see *Section 2.14*). The matrix volume fraction for microscale analysis is evaluated as explained in *supplementary information* (*Section 2.10*).

The elastic modulus of the LMW chitosan film obtained from the tensile test (see Table 1) is used as the matrix property. However, the fiber property are taken from the elastic modulus of the impregnated flax fiber (LMW laminate) obtained from nanoindentation (see *Section 3.2.3)* and applied in the homogenization framework. Later these properties are applied in four-point bending simulation as described in *supplementary information* (*Section 2.17*).

2.5.6.1. Quantification on directional dependency of Young's modulus.

After computation of effective elastic stiffness tensor (4th order), $\overline{\mathbb{C}}$ the variation of young's modulus as a function of direction of load vector $\boldsymbol{d}$ can be calculated as [51]

$$\overline{E}(\boldsymbol{d}) = \left(\overline{\mathbb{C}}^{-1} \cdot \boldsymbol{d}^{\otimes 4}\right)^{-1} \tag{1}$$

where, E is the elastic modulus as a function of direction vector, $\boldsymbol{d}$ and $\mathbb{C}$ is the effective elastic stiffness tensor evaluated at microscale and mesoscale. The scalar product of the fourth order tensor is represented by $(\cdot)$.

An isotropic stiffness tensor $(\mathbb{C}_{iso})$ can be approximated to quantify the directional dependency of elastic modulus which is given as:

$$d = \frac{\|\overline{\mathbb{C}} - \mathbb{C}_{iso}\|}{\|\mathbb{C}_{iso}\|} \times 100 \tag{2}$$

where, the Frobenius norm of the fourth order tensor is given as $\|\mathbb{C}\| = \sqrt{C_{ijkl}C_{ijkl}}$ and

$$\mathbb{C}_{iso} = (\overline{\mathbb{C}} \cdot \mathbb{P}_1)\mathbb{P}_1 + \frac{1}{5}(\overline{\mathbb{C}} \cdot \mathbb{P}_2)\mathbb{P}_2$$

$\mathbb{P}_1$ and $\mathbb{P}_2$ are projection tensors which are orthogonal to each other and they are defined in terms of second order and fourth order symmetric identity tensors, $\boldsymbol{I}$ and $\mathbb{I}^s$ respectively.

$$\mathbb{P}_1 = \frac{1}{3}(\boldsymbol{I} \otimes \boldsymbol{I}) \quad \mathbb{P}_2 = \mathbb{I}^s - \mathbb{P}_1$$

The above written equations are explained in more details in *supplementary information* (*Section 2.18*).

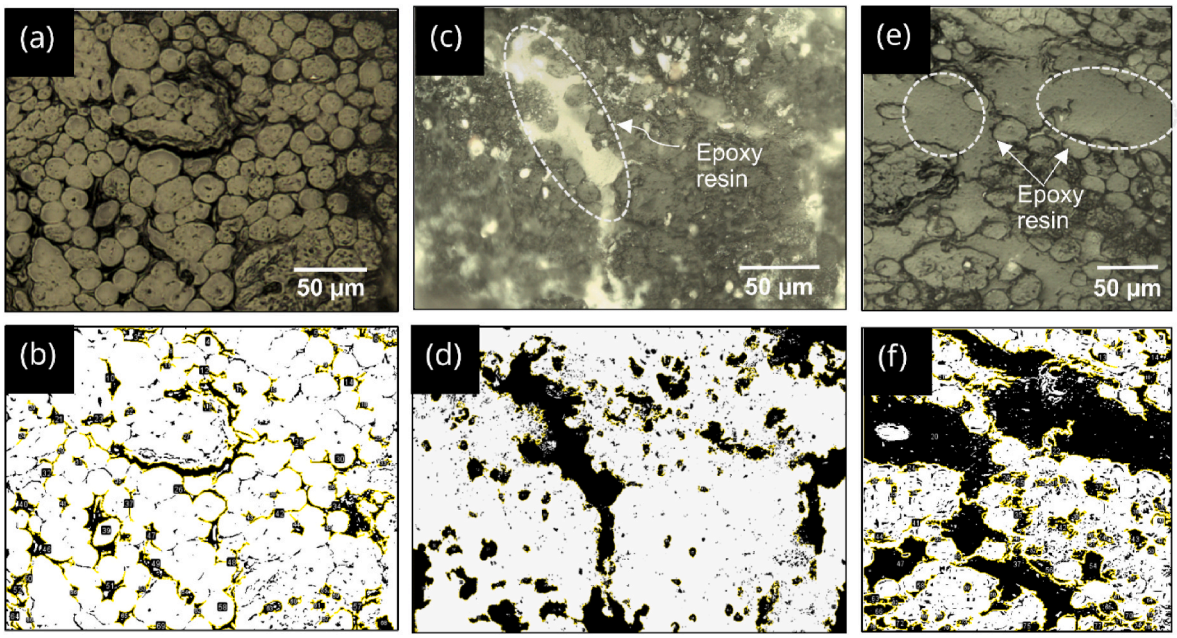

Fig. 5. Microscope images in reflectance showing fibers, matrix and void regions for (a) low molecular weight laminate, (c) medium molecular weight laminate, (e) high molecular weight laminate along with their corresponding binary image product after threshold operation as shown in (b), (d) and (f), respectively. Binary images showing black regions are considered for void area calculation.

Table 1
Summary of material properties obtained from tensile experiment.

Films (F)/ Laminates (L)	Material Density (kg m-3)	Tensile Modulus (GPa)	Ultimate Strength (MPa)	Yield Strength (MPa)	Toughness (J m-3)	Max Elongation (%)	Fiber Volume Fraction (%)
LMW F	1205	5.78 ± 0.30	75.58 ± 2.56	70.95 ± 2.37	182.68 ± 65.80	3.22 ± 1.00	–
MMW F	1304	5.42 ± 0.63	80.26 ± 1.07	75.66 ± 1.77	479.72 ± 179.50	6.93 ± 2.28	–
HMW F	1539	7.98 ± 0.35	94.13 ± 2.22	87.54 ± 2.63	618.17 ± 269.18	6.68 ± 2.30	–
LMW L	1083	6.29 ± 0.88	48.77 ± 4.05	39.39 ± 4.92	47.55 ± 5.53	1.42 ± 0.11	35.54 ± 1.30
MMW L	1182	5.04 ± 0.76	39.60 ± 6.30	33.23 ± 3.81	30.78 ± 7.90	1.22 ± 0.13	31.99 ± 4.53
HMW L	1123	1.61 ± 0.13	15.57 ± 1.20	11.82 ± 0.62	53.54 ± 11.06	4.19 ± 0.69	16.56 ± 0.90

3. Results and discussion

3.1. Effect of molecular weight in laminate fabrication

The final drying process takes about 5–7 days to obtain the final laminates (see Fig. 2). As the viscosities of MMW and HMW are significantly higher than LMW chitosan solution, the concentration of chitosan in the prepared solution is decreased for improved handling during the solvent casting phase. It is important to allow a slow drying process in order to obtain better impregnation on both sides of the flax mat as shown in Fig. 2a and *b*. A faster drying process, e.g. inside a fume hood or an oven can induce warping in the laminates as well as improper fiber impregnation (see Fig. S12).

By slow drying the warping of the sample can be substantially minimized (see also *supplementary information, Section 2.11*).

Chitosan, which is structurally similar to cellulose present in the flax fiber can form a strong interaction through their functional groups. Functional groups present in chitosan are amino-groups (NH2) and hydroxyl-groups (OH), while cellulose has only OH group. The possible chitosan-cellulose interaction between these functional groups are through hydrogen bonds and van der Waals forces, thus forming a strong interface [34,52] as shown in Fig. S13. The formation of a strong interfacial connection depends on the capability of the chitosan solution to penetrate and wet the fibers. Therefore, a LMW solution with low weight-percentage was chosen for the initial step of the fiber impregnation process. The effect of the molecular weight during the solvent casting stage has been studied by casting LMW, MMW and HMW chitosan solutions. The HMW chitosan solution does not wet the pores in the fiber mat owing to very high viscosity of the solution as shown in Fig. 2f. As a result from the optical images that LMW and MMW solutions are suitable for the chitosan-flax composite fabrication process. The desired coating on both sides of the fiber mat turned out to be possible with LMW and MMW chitosan solution (see below for characterization).

3.2. Mechanical testing

3.2.1. Tensile properties

The tensile properties of pure chitosan films and chitosan-flax composite impregnated with different MW chitosan are presented in Table 1. The results show that the tensile modulus of LMW and MMW films are similar with 5.78 ± 0.30 GPa and 5.42 ± 0.63 GPa, respectively, whereas a higher modulus of 7.98 ± 0.35 GPa was measured for HMW films. The average ultimate strength for LMW, MMW and HMW films were found to be 75.58 ± 2.56 MPa, 80.26 ± 1.07 MPa and 94.13 ± 2.22 MPa. The corresponding stress-strain plots of different films are shown in Fig. 3a. A percentage of maximum elongation at the time of fracture for MMW and HMW films were determined to be 6.93 ± 2.28% and 6.68 ± 2.30%, which is twice the value of LMW films with 3.22 ± 1.00%. The higher elongation can be explained due to longer polymer chains along with a higher degree of entanglement. This means the

longer chains can elongate and absorb more energy before they fail as reflected in the toughness of the polymers [53]. The measured toughness for LMW, MMW and HMW films were 182.68 ± 65.80 J m^{-3}, 479.72 ± 179.50 J m^{-3} and 618.17 ± 269.18 J m^{-3}.

The derived tensile modulus of the chitosan films are much higher compared to any other commonly used bio-based polymer or synthetic polymer matrices which are applied in green-composites, such as, polylactic acid (PLA, 0.35–3.50 GPa) [54], polybutylene succinate (PBS, 0.72 GPa) [18], polycaprolactone (PCL, 0.38–0.43 GPa) [55], biobased epoxy resins (3.20–3.40 GPa) [56], polypropylene (PP, 0.68–3.60 GPa) [57], synthetic epoxy resins (3.00–6.00 GPa) [58], polycarbonate (PC, 2.35–2.40 GPa) [59]. Moreover, the moduli of the different MW chitosan films are higher compared to other reported values for chitosan films in the literature (see Table S6).

The tensile modulus of LMW and MMW laminates are 6.29 ± 0.88 GPa and 5.04 ± 0.76 GPa, which is much higher as compared to HMW laminates having a modulus value of 1.61 ± 0.13 GPa (see Table 1 and Fig. 3b). A similar trend in their ultimate strength has been recorded with a value of 48.77 ± 4.05 MPa, 39.60 ± 6.30 MPa and 15.57 ± 1.20 MPa for LMW, MMW and HMW laminates.

This could be attributed to the influence of the MW of the polymer during the impregnation process. This confirms that LMW and MMW chitosan solutions can result in an effective impregnation of the fibers, resulting in a transfer of load from matrix to fibers as reflected in their mechanical properties. In case of the HMW laminates, even though the films show higher modulus and strength, their laminates have poor mechanical properties as a result of improper impregnation due to the highly viscous solution. The strength of the laminates was measured to be considerably lower as compared to pure films which can be attributed to presence of defects in the form of porosity in the composites.

The percentage of maximum elongation has been measured for both pure films as well as their composites. It has been observed that the maximum elongations of LMW and MMW laminates with 1.42% and 1.22% are much lower than the ones of the pure matrix with 3.22% and 6.93%. This can be related to the high porosity of the laminates and undulation of the fibers in a weave that reduces the maximum elongation. Since the load on fibers is locally not parallel to the fibers, it leads to breakage at lower forces.

With this type of fabrication process and based on the geometrical considerations, the maximum fiber volume fraction achieved for tensile specimen is 35.54%, 32.00% and 16.56% for the LMW, MMW and HMW laminate. For bending specimens it is 43.35%, 39.64% and 27.29%, respectively (See *supplementary information*, *Section 2.10* for calculation). Also, a comparison between single and double layer LMW laminate tensile properties has been made so as to examine the effectiveness of load transfer by applying chitosan as a glue for double layer laminate as discussed in *supplementary information* (see *Section 2.8*, Fig. S10 and Table S9). The results from one-way ANOVA indicates that the means between these two groups for tensile modulus and ultimate strength are statistically insignificant.

3.2.2. Flexural properties

A flexural bending test was performed on the LMW, MMW and HMW laminates (see Fig. 3c). A summary of the material properties obtained from the tests for different sample types is mentioned in Table 2.

Table 2
Summary of material properties obtained from bending experiment.

Laminate Type	Flexural Modulus (GPa)	Ultimate Strength (MPa)	Specific Modulus (MNm/kg)	Specific Strength (kNm/kg)	Fiber Volume Fraction (%)
LMW	5.74 ± 0.65	75.54 ± 9.27	5.29 ± 0.64	69.90 ± 5.56	43.35 ± 3.37
MMW	4.06 ± 0.33	89.59 ± 13.41	4.12 ± 0.51	90.21 ± 11.20	39.64 ± 1.79
HMW	3.27 ± 0.05	90.29 ± 11.88	3.52 ± 0.20	94.34 ± 6.76	27.29 ± 2.12

The effect of the MW on the impregnation is also reflected in the flexural testing. The modulus is higher for the LMW laminates compared to the MMW and HMW laminates. The ultimate bending strength is observed to be much higher compared to the tensile strength of all the laminates (70%, 140% and 480% for LMW, MMW and HMW laminates). One of the possible reasons might be the presence of higher fiber volume fractions in the bending samples (43.35% vs 35.54%, 39.64% vs 32.00%, 27.29% vs 16.56% for LMW, MMW and HMW laminates). Despite of the poorly impregnated HMW laminates, its higher bending strength could be attributed to the fact that the sample exhibited a thicker HMW layer on its top which could not pass the weave. This layer can take up load when subjected to tensile stresses during bending. The ultimate tensile strength of pure matrix material is 94.13 MPa for HMW films i.e. in a similar range of the ultimate bending strength of 90.29 MPa.. Another justification for higher bending properties is that the nature of the stresses and strain states in tension and bending are not the same.

During a tensile test, the maximum tensile stresses are experienced throughout the entire volume, while in bending, the maximum tensile stresses and the corresponding compression stresses are rather concentrated in a small region. As a result, the percentage of porosity: 2.41%, 9.54%, 44.48% for LMW, MMW and HMW laminates obtained from μ-CT analysis are observed to be highly sensitive to properties measured in tensile tests than the corresponding properties in bending.

Flexural modulus and strength are not basic material properties, rather than combined effects of a material's tensile, compressive and interlaminar shear properties. Material failure is dictated by the first stress value to be exceeded. In a fiber-matrix composite, the interface is the weakest part of the composite [60]. Thus, the failure mode occurring in a bending test would provide an estimate of the interface condition.

In this study, the failure behavior of three types of laminates are being analyzed visually as well as with an scanning electron microscope. The longitudinal matrix cracks propagating through the fibers along the direction of the applied load appear on the tensile surface of the specimen (see Fig. S15). The surface cracks were found to be sharp and straight implying that the matrix failed in a brittle mode. Such failures are indicative of the flexural tensile type, indicating a strong interfacial interaction between the fibers and the matrix. SEM images of the fractured surfaces are shown in Fig. 4. Chitosan has covered the flax fiber completely as shown in Fig. 4b, c and 4e. This suggests sufficient flow and impregnation of the fiber by chitosan solution potentially contributing to the strong interfacial bonding. It can be seen that some residue of chitosan has been adhered to the surface of the flax fibers which could be pulled out entirely during fracture induced by a bending load. This suggests that the interfacial adhesion is stronger than the strength of the matrix itself. This has been observed for all three different MW laminates as shown in Fig. 4a, d and 4f.

In contrast to chitosan-flax composites, carbon fiber composites or synthetic polymer based natural fiber composites are observed to fail at the compression surface [61]. This compressive failure is associated with the local buckling (microbuckling) of individual fiber due to debonding at the interfacial region [60]. The specimens did not fail catastrophically after reaching the maximum load (see Fig. S15). The measured stress-strain curves (see Fig. 3c) show that the fibers were able to transmit forces even after initial appearance of cracks on the surface between 1% and 2% of strain. This could be attributed to the high percentage elongation of pure films measured from tensile tests (see Table 1). As a result, such type of composites can be envisioned to be used for applications with high impact force without resulting in catastrophic failure.

The Ashby plots (see Figure S8a and S8b) show that strength and modulus of LMW and MMW laminates are in the range of other reported bio polymer and synthetic polymer composites, such as PLA-Flax [41] and Epoxy-Banana fibers [37]. In terms of density variation, LMW and

MMW laminates are 15% and 7.6% lighter in comparison with Epoxy-Banana and PLA-Flax composites. A comparison of tensile strength, flexural modulus and density of different composites are shown in Table S4.

A clear competitive advantage exists for chitosan-flax composites compared to state of the art bio composites due to high modulus and the thermal stability. It shows that LMW and MMW chitosan-flax laminates are superior compared to PLA-Flax, while they are comparable to other synthetic and natural fiber composites. As all the raw materials utilized for fabricating chitosan-flax composites are sustainable, they are suitable composites for future light construction. The raw materials being from renewable sources will not add CO_2 to the atmosphere after biodegradation. However, the processing involved during fabrication will contribute to it. The embodied energy of the processing performed in this manuscript has been calculated to be 74 MJ kg^{-1} (see *supplementary information*, *Section 2.7*).

3.2.3. Chitosan-flax indentation properties

Nanoindentation is a technique to investigate the in-situ mechanical properties at the micron or sub-micron scale without sacrificing the material. It was performed on the lateral cross-section of chitosan-flax composite in order to characterize their spatial nano-mechanical properties (see Fig. S11). The average indentation modulus of impregnated fiber in LMW, MMW and HMW laminate was determined to be 11.13 ± 1.02 GPa, 10.36 ± 0.96 GPa and 9.62 ± 1.27 GPa. The indentation moduli of the matrix were 5.64 ± 0.03 GPa (LMW laminate), 5.32 ± 0.05 GPa (MMW laminate) and 6.04 ± 0.06 GPa (HMW laminate).

It was found that the tensile modulus of pure films (LMW: 5.78 ± 0.30 GPa, MMW: 5.42 ± 0.63 GPa) and the indentation modulus of the matrix are comparable, except for HMW films. The tensile modulus for HMW films (7.98 ± 0.35 GPa) is 33.3% higher as compared to the indentation modulus (6.04 ± 0.06 GPa), which could have raised due to the presence of humidity in the sample during the indentation tests, causing reduction in the values. The yield strength (Y) and martens hardness (H) were shown to be related as $H = 3Y$ for fully plastic deformation in metals, which holds well for polymers as per Tabor's relation [62]. Our studies show that the hardness value obtained from indentation and yield strength from tensile strength to be comparable as per the given relation with a variation of 20.45%, 18.00% and 17.49% for LMW (H: 267.60 ± 6.17 MPa; 3Y: 212.86 ± 7.10 MPa), MMW (H: 276.49 ± 10.04 MPa; 3Y: 226.98 ± 5.31 MPa) and HMW (H:318.30 ± 4.97 MPa; Y: 262.63 ± 7.89 MPa) films, respectively. Nanoindentation could be a valuable technique to predict the strength from the hardness in a nearly non-destructive way.

3.3. Thermal, water content and chemical characterization

The thermal behavior of all pure films (see Fig. S6a) was investigated by DSC. It indicates an endothermic peak associated with the loss of moisture and volatile solvents [63] occurring at ~ 125 °C for LMW and MMW films and at ~100 °C for HMW films. By thermogravimetric analysis (see *supplementary information*, *Section 2.2)* the weight loss of water/acetic acid was determined to be 10.14%, 7.63% and 10.81% at 150 °C for LMW, MMW and HMW films (see Fig. S5). The second observed peak is exothermic and is attributed to a complex process of decomposition of the acetylated and deacetylated units of the polymer occurring at ~260–280 °C for all films. The heat for decomposition appears to be dependent on the MW of the sample showing an increasing trend with higher MW. In the second cycle of heating no major peaks appears on the curve due to decomposition of the sample. This indicates an absence of glass transition (T_g) and melting point temperature (T_m) for chitosan films which are reversible thermal events.

DSC plots for different chitosan-flax laminates are shown in Fig. S6b. The first endothermic peaks related to the release of entrapped moisture appear to be broader as compared to pure films, varying in the range between 100 and 150 °C for all laminate types. Another striking feature of all the laminates is the shifting of the decomposition temperature to a higher temperature range of 320–360 °C which corresponds to an increase of 33.30% compared to chitosan films. The decomposition in this region is due to the thermal depolymerization of hemicellulose and the glycosidic linkages of cellulose present in the fibers [64], thus indicating a higher thermal stability of chitosan-flax composites compared to chitosan films.

The presence of different functional groups in pure films, laminates and flax fibers are characterized in detail by using FTIR spectroscopy. The results show combination of peaks between the functional groups of chitosan and flax (Flax exhibited peaks at 1016 cm^{-1}, 1157 cm^{-1}, 1736 cm^{-1}, 2916 cm^{-1}, and 3300 cm^{-1} representing C–O, C–O–C, C═O, C–H, and OH stretching, respectively. Chitosan exhibited peaks at 1641 cm^{-1}, 1549 cm^{-1}, 1406 cm^{-1}, 1153 cm^{-1}, and 1013 cm^{-1} representing $NHCONH_3$ stretching, $–NH_2$ stretching, CH_3 bending, C–O–C stretching and C-OH bending vibration, respectively), thus confirming the formation of the composite (see *supplementary information*, *Section 2.4* 2.4). The optical transparency (90% in the visible range) of different MW chitosan films was confirmed by UV–Visible spectroscopy (see *supplementary information* Fig. S4 and *Section 2.1*).

3.4. Porosity analysis of chitosan-flax

The performance of composite materials can suffer from process induced defects such as porosity, misalignment of fibers, shape distortion, delamination or undulation. As the viscosities between different MW chitosan vary significantly, their effect on the porosity is a critical parameter. The voids were characterized with the aid of two different techniques: optical microscopic investigation and μ-CT analysis. Characterization using optical imaging technique were performed on the polished samples. (see *supplementary information, Section 1.3*). The porosities were measured to be 10.71%, 21.21% and 43.20% for LMW, MMW and HMW laminates, respectively as shown in Fig. 5.

The porosity calculation from μ-CT analysis shows porosity over three-dimensional volumes, which is more representative compared to images. Fig. 6a1, 6b1 and 6c1 shows a two-dimensional cross-sectional top view and Fig. 6a2, 6b2 and 6c2 the corresponding side view of μ-CT scan reconstruction of fibers, matrix and pores for LMW, MMW and HMW laminates. The three-dimensional view of all the laminates are shown in Fig. 6a3, 6b3 and 6c3. The porosity has been calculated to be 2.41%, 9.54% and 44.48% for LMW, MMW and HMW laminate. The porosity increases with the MW of the chitosan.

The sphericity vs count of the pores is quantified as shown in Fig. 6d. It shows the gaussian plots for the sphericity for LMW and MMW laminate with a mean value of 0.35 and 0.39. This indicates the formation of slit pores for LMW and MMW laminate which can be observed between the stacks of the individual fibers as well as between cross-sectional area of bi-directional fibers.

The amount of pores for MMW laminate is observed to be three times higher compared to LMW laminates. The smaller pore volume as well as the smaller pore count of the LMW laminate can be associated with an effective initial impregnation of fibers and solvent casting. However, the increase in the number of pores for MMW laminates likely originates from solvent casting step due to the higher viscosity of the solution. This has been visually observed for HMW laminates where a much higher viscous chitosan solution was casted during the second step. It is to be mentioned that, with this method the pore count could not be performed for HMW laminate in a similar way as all the smaller pores appear to be connected to form bigger and open volume pore resulting in a single pore count. Thus, it can be inferred that the MW of chitosan has a strong influence on the impregnation stage to control the formation of porosity during the composite fabrication.

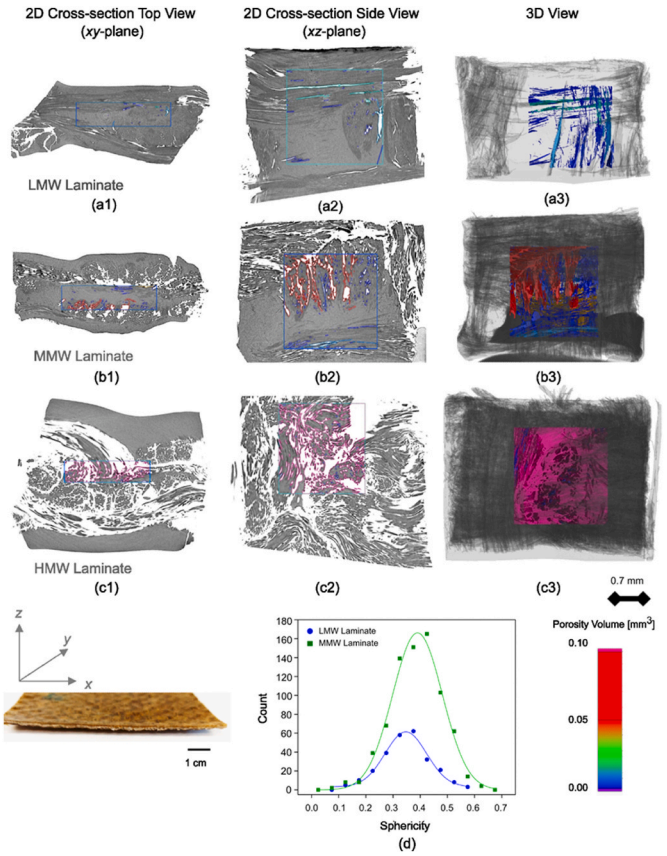

Fig. 6. μ-CT images showing 2D cross-sectional top view of (a1) LMW, (b1) MMW and (c1) HMW laminate; 2D cross-sectional side view of (a2) LMW, (b2) MMW and (c2) HMW laminate; the 3D view of (a3) LMW, (b3) MMW and (c3) HMW laminate; and the (d) gaussian distribution for sphericity of the entrapped pores (slit pores) for LMW and MMW laminate as obtained from micro CT-scan analysis.

3.5. Effective properties of plain weave composite

3.5.1. Two scale homogenization framework

Fig. 7b shows the resulting mesoscale geometry considering certain assumptions (see *supplementary information, Section 2.15*). The effective elastic properties obtained from homogenization methods for microstructure and mesostructure are given in Table 3. The outcome of the effective stiffness based on the homogenization of the microstructure is given as an input for calculating the stiffness of the weave in the mesostructure. Fig. 7d and e shows the variation the elastic modulus E as a function of the direction vector $\boldsymbol{d}$ (see *Section 2.5.6.1*, equation (1)) for effective stiffness obtained at microscale and mesoscale, respectively. In case of the microscale analysis on the fiber plane (*xy*-plane) and normal to the fiber plane (*xz*-plane), it can be observed that the elastic modulus variation is nearly the same and is not strongly direction dependent.

Evaluating equation (1), it is computed that at the microscale, $d =$ 0.25% and hence the effective stiffness is weakly direction dependent. This is very low in comparison to composites in real use [65]. This is due to low contrast ratio (1.93 ± 0.20) in elastic modulus between the fiber (11.13 ± 1.02 GPa) and the matrix (5.78 ± 0.30 GPa). However, at mesoscale it can be noticed that E as a function of $\boldsymbol{d}$ on the fiber mat plane (z-plane) and normal to the fiber mat plane (x-plane) lies around the modulus of an isotropic approximation. The directional dependency of effective stiffness is found to be $d = 2.7\%$.

The effective Young's modulus for LMW laminate (5.96 GPa) obtained from tensile test has been compared with mesoscale effective stiffness in the direction E_{xx} (7.55 GPa). As observed, a 21% higher stiffness value is predicted from the simulation. The effect of high contrast ratio (12.11) on anisotropy is detailed in the *supplementary information* (*Section 2.19*). The obtained effective stiffness value at mesoscale is used in a four-point bending simulation. This is applied to exemplify the utility of the homogenization framework for assessing structural behavior of laminates at macroscale. Fig. 7f shows the force-displacement curve obtained from the FE simulation compared with the experimental data obtained in the linear regime from flexural bending tests. As expected, the simulated plot indicates an overestimated stiffness by showing a higher slope compared to the experimental plot. It is observed for both elastic properties on a structural level from force-displacement curve (geometry dependent) as well as effective stiffness at macroscale (geometry independent) to predict an over-stiff behaviour. The reason for this might be the porosity of 10.71% at microscale (in the orders of micrometres) (see Fig. 5a) which affects the stiffness on mesoscale through the mean behaviour. In addition to this, the porosity of 2.41% (as observed from μ-CT analysis) at mesoscale (in the orders of millimeters) contributes in reduction of the effective behaviour. The superimposed effect of porosity at different length scales gets carried over to macroscale through mean values, which has been neglected in simulation, thus resulting in stiffer prediction.

This modelling approach indicates the possibility to improve the elastic modulus of the laminates by a maximum of 21% through adopting an ideal fabrication technique. This can be reached to certain extent by improving the fabrication process, e.g. either improved impregnation technique or conditions for casting, with the objective of reducing the percentage of porosity at both micro-as well as mesoscale. This topic is beyond the scope and interest of this paper as attention has been paid on establishing a fabrication technique for chitosan-flax composite as a proof-of-principle.

4. Conclusions and outlook

The detailed fabrication technique for chitosan-flax composite and the effect of polymer molecular weight, polymer weight percentage as well as drying conditions were highlighted and discussed. It was concluded that the best impregnation of the flax fibers can be achieved with LMW in the initial impregnation stage followed by applying LMW chitosan solution in the second stage of solvent casting. The highest values for chitosan-flax composite's tensile modulus and strength are 9.0 and 1.8 times, respectively higher in comparison to the chitosan/natural fiber composites reported in the literature before. In addition, flexural properties are reported here for the first time.

Even though the tensile modulus of HMW chitosan films (7.98 GPa) were higher as compared to LMW (5.78 GPa) and MMW films (5.42 GPa), the higher viscosity of the HMW solution prevented a sufficient impregnation of the fibers. The effectiveness of impregnation was reflected in the porosity formation and its subsequent effect on the mechanical performance. The percentage of porosity was evaluated from μ-CT analysis and found to be increasing with increasing MW of the laminate. This effect was reflected in both the tensile as well as the bending properties evaluation with reduction in its properties with increasing MW. The bending properties were evaluated to be higher as compared to tensile properties due to the difference in the nature of stresses and strains. The porosity was observed to be more sensitive for properties measured in tensile than the corresponding properties in bending. It was observed that the strength and modulus particularly of LMW and MMW laminates were in the range of other reported biopolymers and synthetic polymers composites, such as PP-Jute, PLA-Flax, PP-Flax and Epoxy-Banana fibers. Moreover, a clear competitive advantage exists for such composites when specific properties were considered due to their lower density in comparison to other composites in use. The light weight composite would help in tackling future requirements such as improving the fuel efficiency in cars. The consistent failure mode from the bending tests provided an indication of a flexural tensile failure behavior for all laminate types, indicating a strong interfacial interaction between chitosan and flax fibers. The fibers were

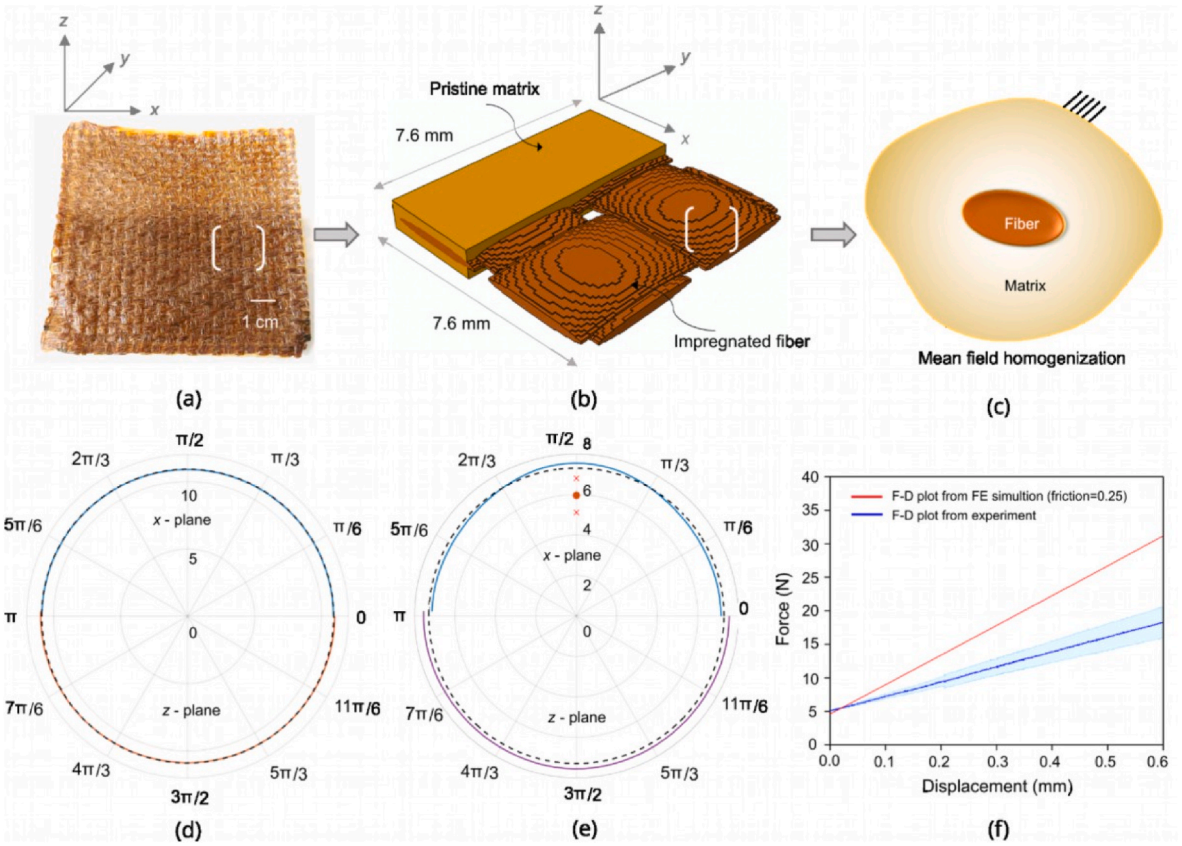

Fig. 7. (a) Macroscale composite structure, (b) mesoscale structure with plane weave, (c) schematic of microstructure used in mean-field homogenization, (d) polar plot of scalar value E as a function of direction of the pull, **d** from microstructural analysis and (e) mesostructural analysis comparing the value with mean tensile modulus for LMW laminate in GPa as indicated by (•) and standard deviation by (×), and (f) load-displacement curve obtained from the FE simulation which is compared with four-point bending measurement for LMW laminate.

Table 3
Effective elastic properties (in GPa) of each flax fabric obtained from mean-field homogenization & full-field homogenization at microscale & mesoscale respectively.

Analysis at	E_{xx}	E_{yy}	E_{zz}	ν_{yx}	ν_{zx}	ν_{xy}	ν_{zy}	ν_{xz}	ν_{yz}	G_{yz}	G_{zx}	G_{xy}
Microscale	10.97	10.88	10.88	0.35	0.35	0.35	0.35	0.35	0.35	4.03	4.04	4.04
Mesoscale	7.55	7.55	7.14	0.32	0.30	0.32	0.30	0.32	0.32	2.69	2.69	2.82

able to transmit forces even after initial indication of cracks on the surface, however there was no catastrophic failure of the composites even after being subjected to maximum load. Thereby providing a dissipating effect. This makes it attractive for high impact loading and energy absorbing applications. Such safety features are short lived or sacrificial which come in handy only during emergency situations. Thus, a fully biodegradable product will be highly beneficial after its end-of-life cycle.

Nano-mechanical properties evaluation was performed to determine the localized modulus of the impregnated fiber region and pure matrix region. These values were incorporated in a combined multiscale homogenization approach to gain an insight into its microscale mechanism, directional dependent behavior of the composite and predicting elastic properties at two length scales. At microscale (in the orders of microns) and mesoscale (in the orders of millimeters), the properties were found to be nearly isotropic with 0.25% and 2.7% directional dependent because of the low elastic contrast between the chitosan and the flax phase of the composite. After assessing the effective stiffness and simulating the structural behavior of four-point bending, an over stiff response is predicted which originates due to neglecting the role of porosity propagating at different length scale as examined experimentally. This provides a scope for improvement by a maximum of 21% of the composite's mechanical properties through reducing the porosity during fabrication stages.

The above study suggests that LMW and MMW laminates can be conveniently envisioned for the applications with low to medium structural load requirements, for e.g., as a replacement material for particle board or plyboard in suspended ceilings, furniture compartments, sports or leisure equipment in the form of skateboards, panels for cargo boxes, etc. Chitosan-flax composites are fully bio-based composite. At the end of the product cycle it additionally offers the possibility either to reenter into the circular economy with the extracted fiber or matrix parts or to be buried in the soil as a fully biodegradable material.

This study provides some design guidelines to consider for manufacturing chitosan-flax composites.

Utilizing such composites is very much in a stage of infancy and further work is needed to test for various applications. Continued research towards this direction will pave the way for future green-based composites as a sustainable alternative to fossil-based products.

Author statement

Amrita Rath: Conceptualization, Visualization, Investigation, Data curation, Methodology, Formal analysis, Writing - original draft.

Benjamin Grisin: Conceptualization, Mechanical properties investigation, Visualization, Resources, Supervision, Writing - review & editing. Tarkes Dora Pallicity: FEA simulation & analysis, Writing – part of original draft, review and editing. Lukas Glaser: Mechanical characterization, Data curation, Writing - review & editing, Jajnabalkya Guhathakurta: μ-CT experiments, Writing – review & editing, Nina Oehlsen: SEM microscopy & Review. Sven Simon: Resources & Review. Stefan Carosella: Resources & Review. Peter Middendorf: Resources & Review. Linus Stegbauer: Conceptualization, Methodology, Formal Analysis, Investigation, Data curation, Visualization, Resources, Validation, Supervision, Writing - review & editing.

Declaration of competing interest

The authors declare that they have no known competing financial interests or personal relationships that could have appeared to influence the work reported in this paper.

Data availability

Data will be made available on request.

Acknowledgements

Generous financial support by the Carl Zeiss Stiftung (Perspectives project ChitinFluid, project P2019-02-004), Fonds der Chemischen Industrie (Fellowship to L.S. and N.O.), German Research Foundation (DFG, AOBJ: 642944) and the European Regional Development Fund (ERDF, FEIH 778511) (for the core facility Stuttgart Research Focus Advanced Materials Innovation and Characterization (AMICA)) is gratefully acknowledged. The authors gratefully acknowledge the core facility SRF AMICA at the University of Stuttgart for their support & assistance in this work. This research also benefitted from the support of CT-Lab Stuttgart with their 3D Analysis capabilities. The authors thank Dr. Thomas Schiestel and Mr. Christopher Hänel from Fraunhofer Institute for Interfacial Engineering and Biotechnology IGB, Mr. Nils von Seggern at Institute for Interfacial Process Engineering and Plasma Technology (IGVP), Mr. Willi Schwan from Institute for Manufacturing Technology of Ceramic Components (IFKB) and Mrs. Dagmar Betsch from Institute of Aircraft Design (IFB), University of Stuttgart for providing access and support in conducting experiments and sample preparation. In particular, we would like to thank Jack Cavanaugh and the referees for their valuable suggestions.

Appendix A. Supplementary data

Supplementary data to this article can be found online at https://doi.org/10.1016/j.compscitech.2023.109952.

References

[1] M.Z. Jacobson, Review of solutions to global warming, air pollution, and energy security, Energy Environ. Sci. 2 (2009) 148–173.
[2] B.P. Chang, A.K. Mohanty, M. Misra, Studies on durability of sustainable biobased composites : a review, R. Soc. Chem. 10 (2020) 17955–17999.
[3] J. Zhang, V.S. Chevali, H. Wang, C. Wang, Current status of carbon fiber and carbon fiber composites recycling, Compos. Part B. 193 (2020), 108053.
[4] K.-Y. Lee, Y. Aitomäki, L.A. Berglund, K. Oksman, A. Bismarck, On the use of nanocellulose as reinforcement in polymer matrix composites, Compos. Sci. Technol. 105 (2014) 15–27.
[5] T. Väisänen, A. Haapala, R. Lappalainen, L. Tomppo, Utilization of agricultural and forest industry waste and residues in natural fiber-polymer composites : a review, Waste Manag. 54 (2016) 62–73.
[6] M. Pervaiz, M.M. Sain, Carbon storage potential in natural fiber composites, Resour. Conserv. Recycl. 39 (2003) 325–340.
[7] E.M. Fernandes, R.A. Pires, J.F. Mano, R.L. Reis, Bionanocomposites from lignocellulosic resources: properties, applications and future trends for their use in the biomedical field, Prog. Polym. Sci. 38 (2013) 1415–1441.
[8] L. Yue, A. Maiorana, A. Patel, R. Gross, I. Manas-Zloczower, A sustainable alternative to current epoxy resin matrices for vacuum infusion molding, Compos. Part A Appl. Sci. Manuf. 100 (2017) 269–274.
[9] S. Rwawiire, B. Tomkova, J. Militky, A. Jabbar, B.M. Kale, Development of a biocomposite based on green epoxy polymer and natural cellulose fabric (bark cloth) for automotive instrument panel applications, Compos. B Eng. 81 (2015) 149–157.
[10] J.J. Andrew, H.N. Dhakal, Sustainable biobased composites for advanced applications: recent trends and future opportunities – a critical review, Compos. Part C Open Access. 7 (2022), 100220.
[11] D.A. Ferreira-Filipe, A. Paço, A.C. Duarte, T. Rocha-Santos, A.L.P. Silva, Are biobased plastics green alternatives?—a critical review, Int. J. Environ. Res. Publ. Health 18 (2021) 7729.
[12] W. Woigk, C.A. Fuentes, J. Rion, D. Hegemann, A.W. Van Vuure, E. Kramer, C. Dransfeld, K. Masania, Fabrication of flax fiber-reinforced cellulose propionate thermoplastic composites, Compos. Sci. Technol. 183 (2019), 107791, https://doi.org/10.1016/j.compscitech.2019.107791.
[13] R.A. Witik, R. Teuscher, V. Michaud, C. Ludwig, J.E. Månson, Carbon fiber reinforced composite waste : an environmental assessment of recycling, energy recovery and landfilling, Compos. Part A Appl. Sci. Manuf. 49 (2013) 89–99.
[14] J. Holbery, D. Houston, Natural-fiber-reinforced polymer composites in automotive applications, J. Miner. Met. Mater. Soc. 58 (2006) 80–86.
[15] J.K. Katiyar, S. Bhattacharya, V.K. Patel, V. Kumar, Automotive Tribology, first ed., Springer Nature, Singapore, 2019 https://doi.org/10.1007/978-981-15-0434-1.
[16] L. Mohammed, M.N.M. Ansari, G. Pua, M. Jawaid, M.S. Islam, A review on natural fiber reinforced polymer composite and its applications, Int. J. Polym. Sci. (2015) 1–15, 2015.
[17] R.A. Ilyas, M.Y.M. Zuhri, H.A. Aisyah, M.R.M. Asyraf, S.A. Hassan, E.S. Zainudin, S. M. Sapuan, S. Sharma, S.P. Bangar, R. Jumaidin, Y. Nawab, A.A.M. Faudzi, H. Abral, M. Asrofi, E. Syafri, N.H. Sari, Natural fiber-reinforced polylactic acid, polylactic acid blends and their composites for advanced applications, Polymers 14 (2022) 202.
[18] A.R. de M. Costa, A. Crocitti, L.H. De Carvalho, S.C. Carroccio, P. Cerruti, G. Santagata, Properties of biodegradable films based on poly(butylene succinate) (PBS) and poly(butylene adipate-co-terephthalate) (PBAT) blends, Polymers 12 (2020) 2317.
[19] E. Vázquez-Núñez, A.M. Avecilla-Ramírez, B. Vergara-Porras, M. del R. López-Cuellar, Green composites and their contribution toward sustainability : a review, Polym. Polym. Compos. 29 (2021) 1588–1608, https://doi.org/10.1177/09673911211009372.
[20] C.P. Jiménez-Gómez, J.A. Cecilia, Chitosan: a natural biopolymer with a wide and varied range of applications, Molecules 25 (2020) 3981.
[21] T. Hahn, E. Tafi, A. Paul, R. Salvia, P. Falabella, S. Zibek, Current state of chitin purification and chitosan production from insects, J. Chem. Technol. Biotechnol. 95 (2020) 2775–2795.
[22] D. Elieh-Ali-Komi, M.R. Hamblin, Chitin and Chitosan: production and application of versatile biomedical nanomaterials, Am. Math. Mon. 4 (2004) 411–427.
[23] P.C. Srinivasa, R. Baskaran, M.N. Ramesh, K.V.H. Prashanth, R.N. Tharanathan, Storage studies of mango packed using biodegradable chitosan film, Eur. Food Res. Technol. 215 (2002) 504–508.
[24] N.A. Qinna, Q.G. Karwi, N. Al-Jbour, M.A. Al-Remawi, T.M. Alhussainy, K.A. Al-So'ud, M.M.H. Al Omari, A.A. Badwan, Influence of molecular weight and degree of deacetylation of low molecular weight chitosan on the bioactivity of oral insulin preparations, Mar. Drugs 13 (2015) 1710–1725.
[25] Chitosan production line offer, n.d. http://www.sumanfoodconsultants.com/pdf/pDF_Chitosan_abstract_ensymm.pdf.
[26] L. Yan, N. Chouw, K. Jayaraman, Flax fiber and its composites - a review, Compos. B Eng. 56 (2014) 296–317.
[27] J.J.E. Hardy, S. Hubert, D.J. Macquarrie, A.J. Wilson, Chitosan-based heterogeneous catalysts for Suzuki and Heck reactions, Green Chem. 6 (2004) 53–56.
[28] A. Dufresne, Processing of polymer nanocomposites reinforced with polysaccharide nanocrystals, Molecules 15 (2010) 4111–4128.
[29] C. Avril, P.A. Bailly, J. Njuguna, E. Nassiopoulos, A. De Larminat, Development of Flax-Reinforced Bio-Composites for High-Load Bearing Automotive Parts, in: ECCM15 - 15th Eur. Conf. Compos. Mater, Venice, Italy, 2012.
[30] T.P. Schlöesser, Natural fiber reinforced automotive parts, in: F.T. Wallenberger, W.N. E (Eds.), Nat. Fibers, Plast. Compos, Springer, Boston, MA, 2004, pp. 275–285.
[31] M.K. Huda, I. Widiastuti, Natural fiber reinforced polymer in automotive application: a systematic literature review, J. Phys. Conf. Ser. 1808 (2021), 012015.
[32] J. Zhu, K. Immonen, C. Avril, J. Brighton, H. Zhu, H. Abhyankar, Novel hybrid flax reinforced supersap composites in automotive applications, Fibers 3 (2015) 76–89.
[33] H.L. Bos, The Potential of Flax Fibers as Reinforcement for Composite Materials, Eindhoven University of Technology, 2004.
[34] M.N. Prabhakar, J. Song, Fabrication and characterisation of starch/chitosan/flax fabric green composites, Int. J. Biol. Macromol. 119 (2018) 1335–1343.
[35] N. Mati-Baouche, H. De Baynast, P. Michaud, T. Dupont, P. Leclaire, Sound absorption properties of a sunflower composite made from crushed stem particles and from chitosan bio-binder, Appl. Acoust. 111 (2016) 179–187.
[36] K.P. Prashanth, S. Sanman, G.N. Lokesh, A Study on tensile and tear properties for chitosan blended with and without natural fiber films, in: C.S. Ramesh, P. Ghosh, E. Natarajan (Eds.), Recent Trends Mech. Eng, Springer Nature, Singapore, 2021.

[37] T.K. Mulenga, A.U. Ude, C. Vivekanandhan, Techniques for modelling and optimizing the mechanical properties of natural fiber composites: a review, Fibers 9 (2021) 1–17.
[38] PP-Flax, n.d. https://www.groupedepestele.com/pro_ecomateriaux_lincoreppang.html.
[39] T.K. Mulenga, A.U. Ude, C. Vivekanandhan, Techniques for modelling and optimizing the mechanical properties of natural fiber composites : a review, Fibers 9 (2021) 6.
[40] W. Gindl-altmutter, J. Keckes, J. Plackner, F. Liebner, K. Englund, M. Laborie, All-cellulose composites prepared from flax and lyocell fibers compared to epoxy – matrix composites, Compos. Sci. Technol. 72 (2012) 1304–1309, https://doi.org/10.1016/j.compscitech.2012.05.011.
[41] J. Inder, P. Singh, S. Singh, V. Dhawan, P. Gulati, Flax fiber reinforced polylactic acid composites for non-structural engineering applications : effect of molding temperature and fiber volume fraction on its mechanical properties, Polym. Polym. Compos. 29 (2021) 780–789, https://doi.org/10.1177/09673911211025159.
[42] No title, n.d. https://www.matweb.com/search/datasheettext.aspx?matguid=39e40851fc164b6c9bda29d798bf3726.
[43] E. Jungstedt, C. Montanari, S. Östlund, L. Berglund, Mechanical properties of transparent high strength biocomposites from delignified wood veneer, Compos. Part A. 133 (2020), 105853, https://doi.org/10.1016/j.compositesa.2020.105853.
[44] F. Chen, D. Sawada, M. Hummel, H. Sixta, T. Budtova, Unidirectional all-cellulose composites from flax via controlled impregnation with ionic liquid, Polymers 12 (2020) 1010.
[45] M. Frey, L. Schneider, K. Masania, T. Keplinger, I. Burgert, Delignified wood–polymer interpenetrating composites exceeding the rule of mixtures, ACS Appl. Mater. Interfaces 11 (2019) 35305–35311, https://doi.org/10.1021/acsami.9b11105.
[46] A.U.M. Shah, M.T.H. Sultan, M. Jawaid, F. Cardona, A.R.A. Talib, A review on the tensile properties of bamboo fiber reinforced polymer composites, Bioresources 11 (2016) 10654–10676.
[47] H.N. Dhakal, M. Sain, Enhancement of mechanical properties of flax-epoxy composite with carbon fiber hybridisation for lightweight applications, Materials 13 (2020) 109.
[48] T. Sonar, S. Patil, V. Deshmukh, R. Acharya, Natural fiber reinforced polymer composite material-A review, IOSR J. Mech. Civ. Eng. (2015) 142–147.
[49] R. Rahman, S.Z.F.S. Putra, Tensile properties of natural and synthetic fiber-reinforced polymer composites, in: M. Jawaid, M. Thariq, N. Saba (Eds.), Mech. Phys. Test. Biocomposites, Fiber-Reinforced Compos. Hybrid Compos, Elsevier Ltd, 2018, pp. 81–102.
[50] A. Courtois, L. Marcin, M. Benavente, E. Ruiz, M. Lévesque, Numerical multiscale homogenization approach for linearly viscoelastic 3D interlock woven composites, Int. J. Solid Struct. 163 (2019) 61–74, https://doi.org/10.1016/j.ijsolstr.2018.12.018.
[51] T. Böhlke, C. Brüggemann, Graphical representation of the generalized hooke's law, Tech. Mech. 21 (2001) 145–158.
[52] H. Zahra, D. Sawada, C. Guizani, Y. Ma, S. Kumagai, T. Yoshioka, H. Sixta, M. Hummel, Close packing of cellulose and chitosan in regenerated cellulose fibers improves carbon yield and structural properties of respective carbon fibers, Biomacromolecules 21 (2020) 4326–4335.
[53] R.A. Chivers, D.R. Moore, The effect of molecular weight and crystallinity on the mechanical properties of injection moulded poly (aryl-ether-ether- ketone) resin, Polymer 35 (1994) 110–116.
[54] D. Tavor, PLA composites reinforced with flax and jute fibers—a review of recent trends, processing parameters and mechanical properties, Polymers 12 (2020) 2373, https://doi.org/10.3390/polym12102373.
[55] M. Wang, X.-Y. Deng, A.-K. Du, T.-H. Zhao, J.-B. Zeng, Poly(sodium 4-styrenesulfonate) modified graphene for reinforced biodegradable poly(3- caprolactone) nanocomposites, RSC Adv. 5 (2015), 73146.
[56] M. Torres-Arellano, V. Renteria-Rodríguez, E. Franco-Urquiza, Mechanical properties of natural-fiber-reinforced biobased epoxy resins manufactured by resin infusion process, Polymers 12 (2020) 2841.
[57] Overview of materials for polypropylene, n.d. https://www.matweb.com/search/DataSheet.aspx?MatGUID=a882a1c603374e278d062f106dfda95b.
[58] N. Sapiai, A. Jumahat, M. Jawaid, M. Midani, A. Khan, Tensile and flexural properties of silica nanoparticles modified unidirectional kenaf and hybrid, Polymers 12 (2020) 2733.
[59] Polymer properties database, n.d. https://polymerdatabase.com/Commercial Polymers/PC.html.
[60] G.C. Shih, L.J. Ebert, Flexural failure mechanisms and global stress plane for unidirectional composites subjected to four-point bending tests, Composites 17 (1986) 309–320.
[61] Q. Wang, W. Wu, Z. Gong, W. Li, Flexural progressive failure of carbon/glass interlayer and intralayer hybrid composites, Materials 11 (2018) 1–18, https://doi.org/10.3390/ma11040619.
[62] D. Tavor, The Hardness of Metals, Oxford University Press, New York, NY, USA, 1951.
[63] F. Ferrero, M. Periolatto, Antimicrobial finish of textiles by chitosan UV-curing, J. Nanosci. Nanotechnol. 12 (2012) 4803–4810.
[64] Z. Dong, R.Y. Ding, L. Zheng, X. Zhang, C.W. Yu, Thermal properties of flax fiber scoured by different methods, Therm. Sci. 19 (2015) 939–945.
[65] L. Kehrer, J.T. Wood, T. Böhlke, Mean-field homogenization of thermoelastic material properties of a long fiber-reinforced thermoset and experimental investigation, J. Compos. Mater. 54 (2020) 3777–3799.